

Bayesian Estimation of Linear Mixtures using the Normal Compositional Model. Application to Hyperspectral Imagery

Olivier Eches, Nicolas Dobigeon,
Corinne Mailhes and Jean-Yves Tourneret

Abstract

This paper studies a new Bayesian unmixing algorithm for hyperspectral images. Each pixel of the image is modeled as a linear combination of so-called *endmembers*. These endmembers are supposed to be random in order to model uncertainties regarding their knowledge. More precisely, we model endmembers as Gaussian vectors whose means have been determined using an endmember extraction algorithm such as the famous N-FINDR or VCA algorithms. This paper proposes to estimate the mixture coefficients (referred to as *abundances*) using a Bayesian algorithm. Suitable priors are assigned to the abundances in order to satisfy positivity and additivity constraints whereas conjugate priors are chosen for the remaining parameters. A hybrid Gibbs sampler is then constructed to generate abundance and variance samples distributed according to the joint posterior of the abundances and noise variances. The performance of the proposed methodology is evaluated by comparison with other unmixing algorithms on synthetic and real images.

Index Terms

Bayesian inference, Monte Carlo methods, spectral unmixing, hyperspectral images, normal compositional model.

I. INTRODUCTION

The spectral unmixing problem has received considerable attention in the signal and image processing literature (see for instance [1] and references therein). Most unmixing procedures for hyperspectral images assume that the image pixels are linear combinations of a given number of pure materials with corresponding fractions referred to as abundances. More precisely, according

The authors are with University of Toulouse, IRIT/INP-ENSEEIHT/TéSA, 2 rue Charles Camichel, BP 7122, 31071 Toulouse cedex 7, France (e-mail: {olivier.eches, nicolas.dobigeon, corinne.mailhes, jean-yves.tourneret}@enseeiht.fr).

to the linear mixing model (LMM) presented in [1], the L -spectrum $\mathbf{y} = [y_1, \dots, y_L]^T$ of a mixed pixel is assumed to be a mixture of R spectra \mathbf{m}_r , $r = 1 \dots R$, corrupted by additive white Gaussian noise

$$\mathbf{y} = \sum_{r=1}^R \mathbf{m}_r \alpha_r + \mathbf{n} \quad (1)$$

where $\mathbf{m}_r = [m_{r,1}, \dots, m_{r,L}]^T$ denotes the spectrum of the r^{th} material, α_r is the fraction of the r^{th} material in the pixel, R is the number of pure materials (or endmembers) present in the observed scene and L is the number of available spectral bands for the image. Supervised algorithms assume that the R endmember spectra \mathbf{m}_r are known, e.g., extracted from a spectral library. In practical applications, they can be obtained by an endmember extraction procedure such as the well-known N-finder (N-FINDR) algorithm developed by Winter [2] or the Vertex Component Analysis (VCA) presented by Nascimento [3]. Due to physical considerations, the abundances satisfy the following positivity and sum-to-one constraints

$$\begin{cases} \alpha_r \geq 0, \forall r = 1, \dots, R, \\ \sum_{r=1}^R \alpha_r = 1. \end{cases} \quad (2)$$

The LMM has some limitations when applied to real images [1]. In particular, the ratio between the intra-class variance (within endmember classes) and the inter-class variance (between endmembers) allows one to question the validity of the deterministic spectrum assumption [4]. Moreover, the endmember extraction procedures based on the LMM can be inefficient when the image does not contain enough pure pixels. This problem, outlined in [3], is illustrated in Fig. 1. This figure shows 1) the dual-band projections (on the two most discriminant axes identified by a principal component analysis (PCA)) of $R = 3$ endmembers (red stars corresponding to the vertices of the red triangle), 2) the dual-band domain containing all linear combinations of the $R = 3$ endmembers (i.e., the red triangle), and 3) the dual-band simplex estimated by the N-FINDR algorithm using the black pixels. As there is no pixel close to the vertices of the red triangle, the N-FINDR estimates a much smaller simplex (in blue) than the actual one (in red).

A new model referred to as normal compositional model (NCM) was recently proposed in [4]. The NCM allows one to alleviate the problems mentioned above by assuming that the pixels of the hyperspectral image are linear combinations of random endmembers (as opposed to deterministic for the LMM) with known means (e.g., resulting from the N-FINDR or VCA algorithms). This model allows more flexibility regarding the observed pixels and the endmembers. In particular,

the endmembers are allowed to be further from the observed pixels which is clearly an interesting property for the problem illustrated in Fig. 1. The NCM assumes that the spectrum of a mixed pixel can be written as follows

$$\mathbf{y} = \sum_{r=1}^R \boldsymbol{\varepsilon}_r \alpha_r \quad (3)$$

where the $\boldsymbol{\varepsilon}_r$ are independent Gaussian vectors with known means, e.g., extracted from a spectral library or estimated by an appropriate method such as the VCA algorithm. Note that there is no additive noise in (3) since the random nature of the endmembers already models some kind of uncertainty regarding the endmembers. This paper assumes that the covariance matrix of each endmember is proportional to the identity matrix. As a consequence, the endmember variances do not vary from one spectral band to another¹.

In this paper, a new Bayesian unmixing algorithm is derived from the NCM to estimate the abundance coefficients in (3) under the constraints in (2). Appropriate prior distributions are chosen for the NCM abundances to satisfy the positivity and sum-to-one constraints, as in [7]. A conjugate inverse Gamma distribution is defined for the endmember variance. The hyperparameter of this model can be fixed using appropriate prior information, or estimated jointly with the other unknown parameters. A classical procedure consists of assigning a vague prior to this hyperparameter resulting in a hierarchical Bayesian model [8, p. 392]. The parameters and hyperparameter of this hierarchical Bayesian model can then be estimated using the full posterior distribution. Unfortunately the joint posterior distribution for the NCM is too complex to derive the standard minimum mean square error (MMSE) or maximum *a posteriori* (MAP) estimators. The complexity of the posterior can be handled by the expectation maximization (EM) algorithm [4], [9]. However, this algorithm can have “*serious shortcomings including the convergence to a local maximum of the posterior*” [10, p. 259]. These shortcomings can be bypassed by considering Markov Chain Monte Carlo (MCMC) methods that allow one to generate samples distributed according to the posterior of interest (here the joint posterior of the abundances and the endmember variance). This paper generalizes the hybrid Gibbs sampler developed in [7] and shows that it can be used efficiently for the NCM. Note that other Bayesian algorithms have been also proposed for multispectral and hyperspectral image analysis.

¹Note that more sophisticated models with different variances in the spectral bands could be investigated. However, the simplifying assumption of a common variance in all spectral bands has been considered successfully in many studies [5], [6].

In [11], Moussaoui *et al.* have coupled Bayesian blind source separation with independent component analysis to investigate the composition of the Mars surface. This approach, relied on MCMC methods, has allowed them to handle the spectral unmixing problem in an unsupervised framework. In [12], classification and segmentation of hyperspectral images have been addressed using a Bayesian model with a Potts-Markov field to take into account spatial constraints. More recently, Snoussi introduced in [13] an MCMC algorithm to extract the cosmic microwave background power spectrum in astrophysical data.

The paper is organized as follows. Section II derives the posterior distribution of the unknown parameter vector resulting from the proposed Bayesian model. Section III studies the hybrid Gibbs sampling strategy that is used to generate samples distributed according to the NCM posterior. Section IV and V extend the proposed result to endmembers with different variances. Simulation results conducted on synthetic data are presented in Section VI. In particular, some comparisons between the proposed Bayesian strategies and classical unmixing algorithms are presented in this Section. Results obtained with these algorithms on a real image are finally presented in section VII. Conclusions are reported in Section VIII.

II. HIERARCHICAL BAYESIAN MODEL

This section studies the likelihood and the priors inherent to the proposed NCM for the spectral unmixing of hyperspectral images. A particular attention is devoted to defining abundance prior distributions satisfying positivity and sum-to-one constraints.

A. Likelihood

The NCM assumes that the endmember spectra $\boldsymbol{\varepsilon}_r$, $r = 1, \dots, R$, are independent Gaussian vectors with known mean vectors $\mathbf{m}_r = [m_{r,1}, \dots, m_{r,L}]^T$, $r = 1, \dots, R$. Moreover, we first assume that the covariance matrix of each endmember can be written $\sigma^2 \mathbf{I}_L$, where \mathbf{I}_L is the $L \times L$ identity matrix and σ^2 is the endmember variance in any spectral band, i.e., $\boldsymbol{\varepsilon}_r | \mathbf{m}_r, \sigma^2 \sim \mathcal{N}(\mathbf{m}_r, \sigma^2 \mathbf{I}_L)$ where $\mathcal{N}(\mathbf{m}, \Sigma)$ denotes the multivariate Gaussian distribution with mean vector \mathbf{m} and covariance matrix Σ . Using (3) and the *a priori* independence between the endmember spectra, the likelihood of the observed pixel \mathbf{y} can be written as

$$f(\mathbf{y} | \boldsymbol{\alpha}^+, \sigma^2) = \frac{1}{[2\pi\sigma^2 c(\boldsymbol{\alpha}^+)]^{\frac{L}{2}}} \exp\left(-\frac{\|\mathbf{y} - \mu(\boldsymbol{\alpha}^+)\|^2}{2\sigma^2 c(\boldsymbol{\alpha}^+)}\right) \quad (4)$$

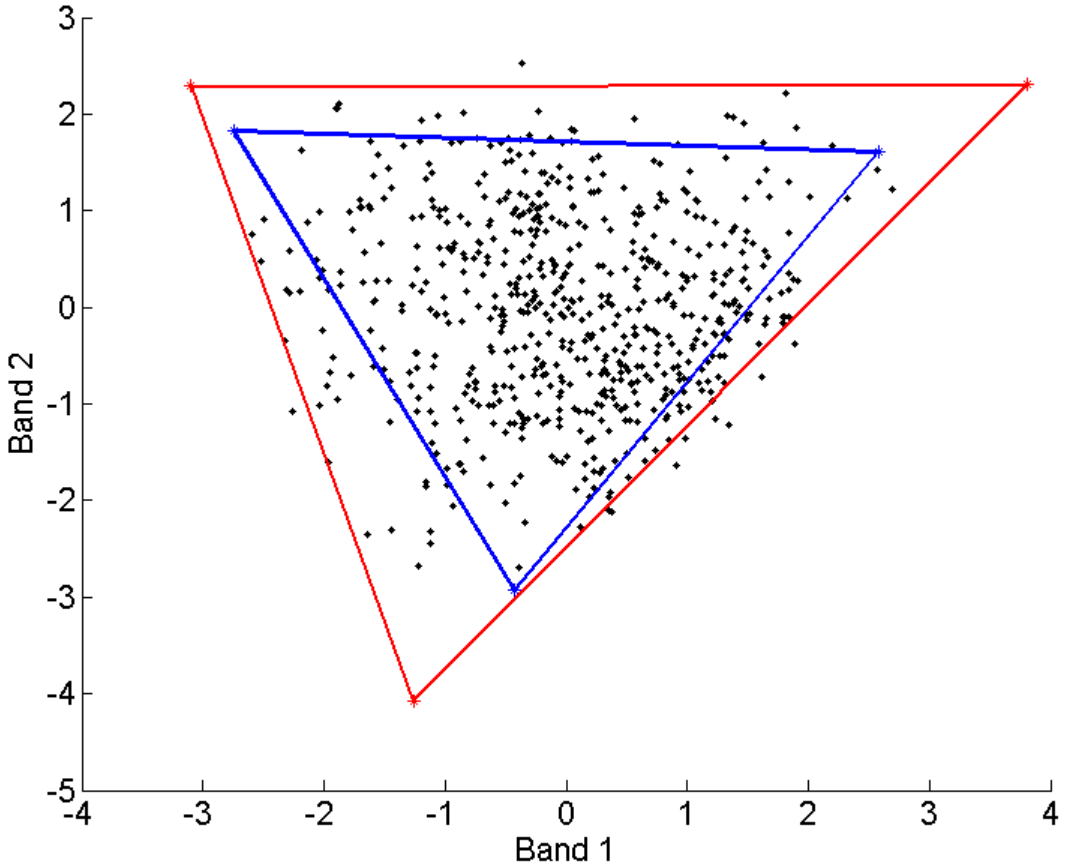


Fig. 1. Scatterplot of dual-band correct (red) and incorrect (blue) results of the N-FINDR algorithm.

where $\|\mathbf{x}\| = \sqrt{\mathbf{x}^T \mathbf{x}}$ is the standard ℓ^2 norm, $\boldsymbol{\alpha}^+ = [\alpha_1, \dots, \alpha_R]^T$, and

$$\mu(\boldsymbol{\alpha}^+) = \sum_{r=1}^R \mathbf{m}_r \alpha_r, \quad c(\boldsymbol{\alpha}^+) = \sum_{r=1}^R \alpha_r^2. \quad (5)$$

Note that the mean and variance of this Gaussian distribution depend both on the abundance vector $\boldsymbol{\alpha}^+$ contrary to the classical LMM.

B. Parameter priors

1) *Abundance prior:* Because of the sum-to-one constraint inherent to the mixing model, the abundance vector can be rewritten as $\boldsymbol{\alpha}^+ = [\boldsymbol{\alpha}^T, \alpha_R]^T$ where $\alpha_R = 1 - \sum_{r=1}^{R-1} \alpha_r$. Moreover, to

satisfy the positivity constraint, the abundance sub-vector α lives in a simplex defined by

$$\mathbb{S} = \left\{ \boldsymbol{\alpha} \mid \alpha_r \geq 0, \forall r = 1, \dots, R-1, \sum_{r=1}^{R-1} \alpha_r \leq 1 \right\}. \quad (6)$$

A uniform distribution on this simplex is chosen as prior distribution for the partial abundance vector α

$$f(\boldsymbol{\alpha}) \propto \mathbf{1}_{\mathbb{S}}(\boldsymbol{\alpha}), \quad (7)$$

where \propto means “proportional to” and $\mathbf{1}_{\mathbb{S}}(\cdot)$ is the indicator function defined on the set \mathbb{S} :

$$\mathbf{1}_{\mathbb{S}}(\boldsymbol{\alpha}) = \begin{cases} 1, & \text{if } \boldsymbol{\alpha} \in \mathbb{S}; \\ 0, & \text{otherwise.} \end{cases} \quad (8)$$

This prior ensures the positivity and sum-to-one constraints of the abundance coefficients and reflects the absence of other prior knowledge regarding these parameters. Note that any abundance could be removed from α^+ and not only the last one α_R . For symmetry reasons, the algorithm proposed in Section III will remove one abundance coefficient from α^+ uniformly drawn in $\{1, \dots, R\}$. Here, this component is supposed to be α_R to simplify notations. Moreover, for sake of conciseness, the notations $\mu(\boldsymbol{\alpha})$ and $c(\boldsymbol{\alpha})$ will be used in the sequel to denote the quantities in (5) where α_R has been replaced by $1 - \sum_{r=1}^{R-1} \alpha_r$.

2) *Endmember variance prior:* The prior distribution for the variance σ^2 is a conjugate inverse Gamma distribution

$$\sigma^2 | \delta \sim \mathcal{IG}(\nu, \delta), \quad (9)$$

where ν and δ are two adjustable hyperparameters (referred to as shape and scale parameters [8, p. 582]). This paper classically assumes $\nu = 1$ (as in [14] or [15]) and estimates δ using a hierarchical Bayesian algorithm. Hierarchical Bayesian algorithms require to define prior distributions for the hyperparameters. This paper assumes that the prior of δ is the non-informative Jeffreys' prior defined by

$$f(\delta) \propto \frac{1}{\delta} \mathbf{1}_{\mathbb{R}^+}(\delta). \quad (10)$$

This prior reflects the lack of knowledge regarding the hyperparameter δ .

C. Posterior distribution of the parameters

The joint posterior distribution of the unknown parameter vector $\boldsymbol{\theta} = \{\boldsymbol{\alpha}, \sigma^2\}$ and hyperparameter δ can be derived using the hierarchical structure

$$f(\boldsymbol{\theta}, \delta | \mathbf{y}) \propto f(\mathbf{y} | \boldsymbol{\theta}) f(\boldsymbol{\theta} | \delta) f(\delta) \quad (11)$$

where $f(\mathbf{y} | \boldsymbol{\theta})$ and $f(\delta)$ have been defined in (4) and (10), respectively. Assuming independence between the unknown parameters, the prior distribution of $\boldsymbol{\theta}$ is $f(\boldsymbol{\theta} | \delta) = f(\boldsymbol{\alpha}) f(\sigma^2 | \delta)$, yielding

$$\begin{aligned} f(\boldsymbol{\theta}, \delta | \mathbf{y}) &\propto \frac{1}{c(\boldsymbol{\alpha}^+)^{\frac{L}{2}}} \frac{1}{\sigma^{L+2}} \\ &\quad \times \exp\left(-\frac{\|\mathbf{y} - \boldsymbol{\mu}(\boldsymbol{\alpha})\|^2}{2\sigma^2 c(\boldsymbol{\alpha})} - \delta\right) \mathbf{1}_{\mathbb{S}}(\boldsymbol{\alpha}) \mathbf{1}_{\mathbb{R}^+}(\delta). \end{aligned} \quad (12)$$

The posterior distribution (12) is too complex to derive the MMSE or MAP estimators of the unknown parameter of interest, i.e, the vector of abundances $\boldsymbol{\alpha}^+$. An interesting alternative is to generate samples distributed according to the posterior and to use the generated samples to approximate the Bayesian estimators [8]. The next section studies a hybrid Gibbs sampler that generates abundances and variances distributed according to the full posterior (12).

III. HYBRID GIBBS SAMPLER

This section studies a hybrid Metropolis-within-Gibbs sampler that generates samples according to the posterior $f(\boldsymbol{\theta} | \mathbf{y})$. The sampler iteratively generates $\boldsymbol{\alpha}$ according to $f(\boldsymbol{\alpha} | \mathbf{y}, \sigma^2)$, σ^2 according to $f(\sigma^2 | \mathbf{y}, \boldsymbol{\alpha}, \delta)$, and δ according to $f(\delta | \sigma^2)$, as detailed below. The overall hybrid Gibbs sampler algorithm is summarized in Algo. 1.

A. Generation according to $f(\boldsymbol{\alpha} | \mathbf{y}, \sigma^2)$

The Bayes' theorem yields

$$f(\boldsymbol{\alpha} | \mathbf{y}, \sigma^2) \propto f(\mathbf{y} | \boldsymbol{\theta}) f(\boldsymbol{\theta}) \quad (13)$$

which easily leads to

$$f(\boldsymbol{\alpha} | \mathbf{y}, \sigma^2) \propto \frac{1}{[\sigma^2 c(\boldsymbol{\alpha})]^{L/2}} \exp\left(-\frac{\|\mathbf{y} - \boldsymbol{\mu}(\boldsymbol{\alpha})\|^2}{2\sigma^2 c(\boldsymbol{\alpha})}\right) \mathbf{1}_{\mathbb{S}}(\boldsymbol{\alpha}). \quad (14)$$

Note that the conditional distribution of $\boldsymbol{\alpha}$ is defined on the simplex \mathbb{S} . As a consequence, the abundance vector $\boldsymbol{\alpha}^+$ satisfies the positivity and sum-to-one constraints. The generation of $\boldsymbol{\alpha}$ according to (14) can be achieved using a Metropolis-within-Gibbs algorithm. We have used the uniform prior distribution (7) as proposal distribution for this algorithm.

B. Generation according to $f(\sigma^2|\mathbf{y}, \boldsymbol{\alpha}, \delta)$

The conditional distribution of the variance σ^2 can be determined as follows

$$f(\sigma^2|\mathbf{y}, \boldsymbol{\alpha}, \delta) \propto f(\mathbf{y}|\boldsymbol{\theta})f(\sigma^2|\delta). \quad (15)$$

Consequently, $\sigma^2|\mathbf{y}, \boldsymbol{\alpha}, \delta$ is distributed according to the following inverse-Gamma distribution

$$\sigma^2|\mathbf{y}, \boldsymbol{\alpha}, \delta \sim \mathcal{IG}\left(\frac{L}{2} + 1, \frac{\|\mathbf{y} - \boldsymbol{\mu}(\boldsymbol{\alpha})\|^2}{2c(\boldsymbol{\alpha})} + \delta\right). \quad (16)$$

C. Generation according to $f(\delta|\sigma^2)$

The conditional distribution of δ is

$$\delta|\sigma^2 \sim \mathcal{G}\left(1, \frac{1}{\sigma^2}\right) \quad (17)$$

where $\mathcal{G}(a, b)$ is the Gamma distribution with shape parameter a and scale parameter b [8, p. 581].

ALGORITHM 1:
Hybrid Gibbs sampler for hyperspectral unmixing using the NMC

- 1) Initialization:
 - Sample $\delta^{(0)}$ from the probability density function (pdf) in Eq. (10),
 - Sample $\sigma^{2(0)}$ from the pdf in Eq. (9),
- 2) Iterations: For $t = 1, 2, \dots$, do
 - Sample $\boldsymbol{\alpha}^{(t)}$ from the pdf in Eq. (14) using Metropolis-within-Gibbs step,
 - Sample $\sigma^{2(t)}$ from the pdf in Eq. (16),
 - Sample $\delta^{(t)}$ from the pdf in Eq. (17),

IV. EXTENSION TO ENDMEMBER SPECTRA WITH DIFFERENT VARIANCES

In the previous sections, all endmembers spectra shared the same variance σ^2 . We propose here to extend the previous model to the case where endmembers have different variances. This additional degree of freedom can be particularly interesting when different levels of confidence are given to the mean vectors \mathbf{m}_r ($r = 1, \dots, R$) identified by the N-FINDR or VCA algorithms. Thus, a new vector $\boldsymbol{\sigma} = [\sigma_1^2, \dots, \sigma_R^2]^T$ is introduced, where σ_r^2 is the r th endmember variance. This assumption leads to

$$\boldsymbol{\varepsilon}_r | \mathbf{m}_r, \sigma_r^2 \sim \mathcal{N}(\mathbf{m}_r, \sigma_r^2 \mathbf{I}_L). \quad (18)$$

A. Identifiability issue

1) *General theory*: If the prior distributions chosen for σ_r^2 ($r = 1, \dots, R$) are not sufficiently informative, indeterminacy issues may occur. In this case, the space to be explored by the MCMC algorithm may be wide, leading to very poor mixing properties of the Gibbs sampler. Indeed, when R endmembers are involved in the mixture, the log-likelihood can be written as follows

$$\log f(\mathbf{y}|\boldsymbol{\sigma}, \boldsymbol{\alpha}) = -\frac{L}{2} \log C(\boldsymbol{\sigma}) - \frac{K(\mathbf{y}, \boldsymbol{\alpha})}{C(\boldsymbol{\alpha}, \boldsymbol{\sigma})} \quad (19)$$

where $K(\mathbf{y}, \boldsymbol{\alpha}) = \frac{1}{2} \|\mathbf{y} - \boldsymbol{\mu}(\boldsymbol{\alpha})\|^2$ and $C(\boldsymbol{\alpha}, \boldsymbol{\sigma}) = \sum_{r=1}^R \sigma_r^2 \alpha_r^2$. Looking for the values of the vector $\boldsymbol{\sigma}$ which maximize the log-likelihood, we equal its R partial derivatives to zero

$$\left\{ \begin{array}{lcl} \frac{\partial \log f(\mathbf{y}|\boldsymbol{\sigma})}{\partial \sigma_1^2} & = & -\frac{L\alpha_1^2}{2C(\boldsymbol{\alpha}, \boldsymbol{\sigma})} - \frac{K(\mathbf{y}, \boldsymbol{\alpha})\alpha_1^2}{[C(\boldsymbol{\alpha}, \boldsymbol{\sigma})]^2} = 0, \\ \vdots \\ \frac{\partial \log f(\mathbf{y}|\boldsymbol{\sigma})}{\partial \sigma_R^2} & = & -\frac{L\alpha_R^2}{2C(\boldsymbol{\alpha}, \boldsymbol{\sigma})} - \frac{K(\mathbf{y}, \boldsymbol{\alpha})\alpha_R^2}{[C(\boldsymbol{\alpha}, \boldsymbol{\sigma})]^2} = 0, \end{array} \right. \quad (20)$$

which easily leads to

$$C(\boldsymbol{\alpha}, \boldsymbol{\sigma}) = \sum_{r=1}^R \sigma_r^2 \alpha_r^2 = \frac{2K}{L}.$$

Consequently, the likelihood $f(\mathbf{y} | \boldsymbol{\sigma}, \boldsymbol{\alpha})$ has several maxima located on the hyperplane \mathcal{H} defined by

$$\mathcal{H} = \left\{ \boldsymbol{\sigma} = [\sigma_1^2, \dots, \sigma_R^2]^T \mid C(\boldsymbol{\alpha}, \boldsymbol{\sigma}) = \frac{2K}{L} \right\}. \quad (21)$$

However, this identifiability issue can be alleviated when several pixels with the same characteristics are considered. Assuming the variance vector $\boldsymbol{\sigma}$ is the same for P pixels (with $P > 1$), a linear system of P equations is obtained

$$\left\{ \begin{array}{l} \sum_{r=1}^R \sigma_r^2 \alpha_{r,1}^2 = \frac{2K_1}{L}, \\ \vdots \\ \sum_{r=1}^R \sigma_r^2 \alpha_{r,P}^2 = \frac{2K_P}{L}, \end{array} \right. \quad (22)$$

where $\alpha_{r,p}$ denotes the abundance of the r th endmember in the p th pixel, $K_p = \frac{1}{2} \|\mathbf{y}_p - \boldsymbol{\mu}(\boldsymbol{\alpha}_p)\|^2$, $\boldsymbol{\alpha}_p = [\alpha_{1,p}, \dots, \alpha_{R-1,p}]^T$ and \mathbf{y}_p is the p th measured spectrum pixel (with $p = 1, \dots, P$). This system can be rewritten as

$$\Lambda \boldsymbol{\sigma} = \frac{2}{L} \mathbf{K}$$

with

$$\boldsymbol{\Lambda} = \begin{pmatrix} \alpha_{1,1}^2 & \cdots & \alpha_{R,1}^2 \\ \vdots & \ddots & \vdots \\ \alpha_{1,P}^2 & \cdots & \alpha_{R,P}^2 \end{pmatrix}, \quad \boldsymbol{K} = \begin{pmatrix} K_1 \\ \vdots \\ K_P \end{pmatrix}. \quad (23)$$

Thus, the vector $\boldsymbol{\sigma}$ maximizing the likelihood is unique provided the rank of the matrix $\boldsymbol{\Lambda}$ is equal to R .

2) *Examples:* We illustrate the identifiability condition when different numbers of pixels are generated from the mixture of $R = 2$ endmembers. As an example, a pixel has been generated with $\boldsymbol{\sigma} = [0.006, 0.002]^T$. Fig. 2 shows the corresponding log-likelihood as a function of (σ_1^2, σ_2^2) for $P = 1$ pixel. This figure clearly shows that the maxima are reached for an infinity of couples (σ_1^2, σ_2^2) located on a hyperplane (here a line).

Fig. 3 shows the likelihood as a function of $\boldsymbol{\sigma}$ for $P = 2$ pixels. A unique maximum can be

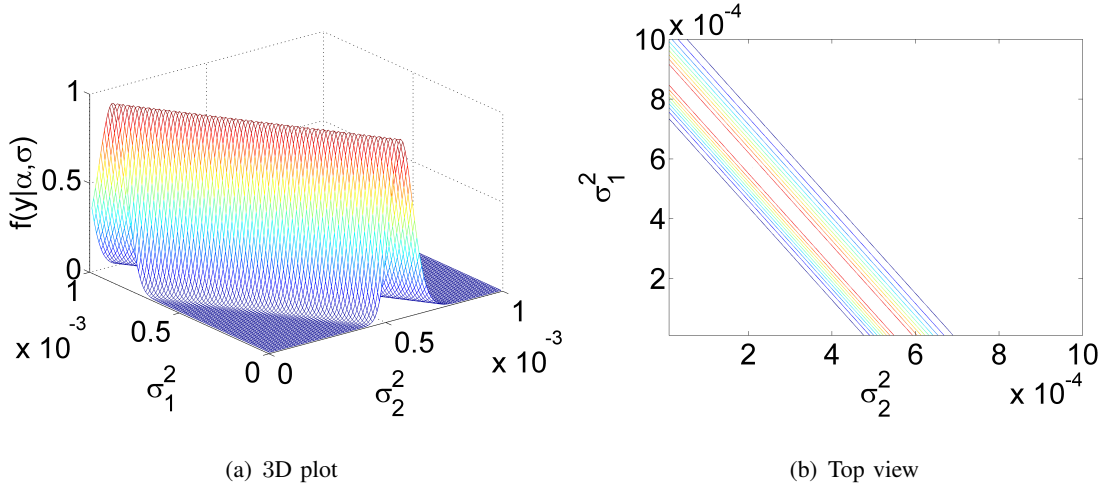


Fig. 2. Likelihood for $P = 1$ pixel as a function of (σ_1^2, σ_2^2) . (a) 3D view. (b) Top view.

observed since the rank of $\boldsymbol{\Lambda}$ equals 2 for this example. The results depicted in Fig. 4 obtained for $P = 9$ pixels show that the likelihood is more peaky around the true value of $\boldsymbol{\sigma}$ when more pixels are considered.

B. Hierarchical Bayesian model

This section derives the hierarchical Bayesian model that can be used to consider different endmember variances σ_r^2 ($r = 1, \dots, R$). Motivated by the considerations of the previous

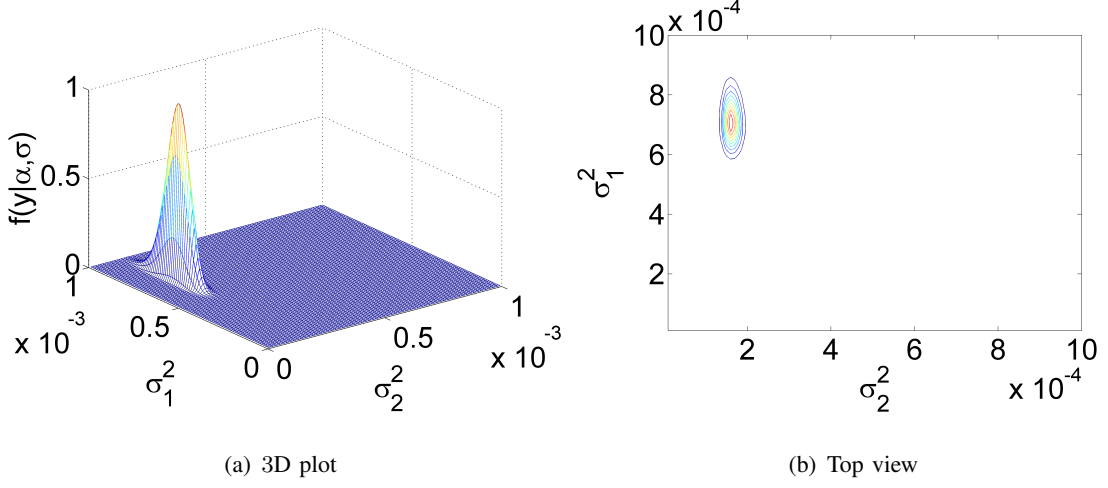


Fig. 3. Likelihood for $P = 2$ pixels as a function of (σ_1^2, σ_2^2) . (a) 3D view. (b) Top view.

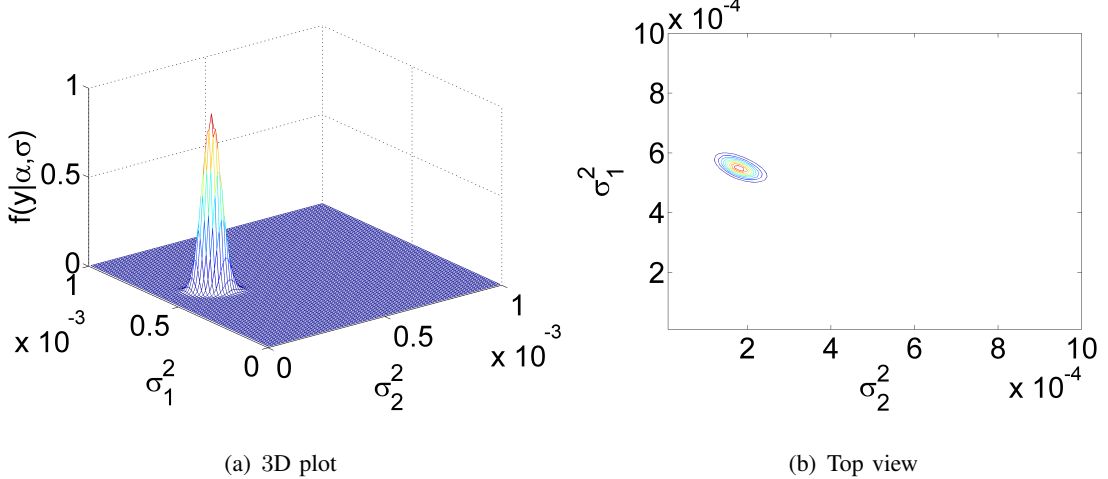


Fig. 4. Likelihood for $P = 9$ pixels as a function of (σ_1^2, σ_2^2) . (a) 3D View. (b) Top view.

paragraph, P pixel spectra are considered:

$$\mathbf{y}_p = \sum_{r=1}^R \boldsymbol{\varepsilon}_r \alpha_{r,p}, \quad p = 1, \dots, P \quad (24)$$

where $\varepsilon_r | \mathbf{m}_r, \sigma_r^2 \sim \mathcal{N}(\mathbf{m}_r, \sigma_r^2 \mathbf{I}_L)$, $\mathbf{m}_r = [m_{r,1}, \dots, m_{r,L}]^T$ represents the known mean vector of the endmember vector ε_r , and $\boldsymbol{\sigma} = [\sigma_1^2, \dots, \sigma_R^2]^T$ is the unknown variance vector. A standard matrix formulation yields

$$Y = EA \quad (25)$$

where

$$\mathbf{Y} = \begin{pmatrix} y_{1,1} & \cdots & y_{1,P} \\ \vdots & \ddots & \vdots \\ y_{L,1} & \cdots & y_{L,P} \end{pmatrix}, \quad \mathbf{E} = [\boldsymbol{\varepsilon}_1, \dots, \boldsymbol{\varepsilon}_R]$$

and

$$\mathbf{A} = \begin{pmatrix} \alpha_{1,1} & \cdots & \alpha_{1,P} \\ \vdots & \ddots & \vdots \\ \alpha_{R,1} & \cdots & \alpha_{R,P} \end{pmatrix}. \quad (26)$$

The corresponding likelihood and prior distributions are described below.

1) *Likelihood*: The likelihood function for the pixel $\#p$ is

$$f(\mathbf{y}_p | \boldsymbol{\alpha}_p, \boldsymbol{\sigma}) \propto \frac{1}{[c(\boldsymbol{\alpha}_p)]^{L/2}} \exp \left[-\frac{\|\mathbf{y}_p - \boldsymbol{\mu}(\boldsymbol{\alpha}_p)\|^2}{2c(\boldsymbol{\alpha}_p)} \right]$$

with

$$\begin{cases} c(\boldsymbol{\alpha}_p) = \sum_{r=1}^R \sigma_r^2 \alpha_{r,p}^2, \\ \boldsymbol{\mu}(\boldsymbol{\alpha}_p) = \sum_{r=1}^R \mathbf{m}_r \alpha_{r,p}. \end{cases} \quad (27)$$

Assuming the pixel spectra \mathbf{y}_p ($p = 1, \dots, P$) are *a priori* independent, the joint likelihood for the set of P pixels can be written

$$f(\mathbf{Y} | \mathbf{A}, \boldsymbol{\sigma}) \propto \prod_{p=1}^P \frac{1}{[c(\boldsymbol{\alpha}_p)]^{L/2}} \exp \left[-\sum_{p=1}^P \frac{\|\mathbf{y}_p - \boldsymbol{\mu}(\boldsymbol{\alpha}_p)\|^2}{2c(\boldsymbol{\alpha}_p)} \right]. \quad (28)$$

2) *Prior distributions*: Uniform distributions on the simplex defined in (6) are chosen as prior distributions for the partial abundance vectors $\boldsymbol{\alpha}_p$ assumed to be *a priori* independent ($p = 1, \dots, P$)

$$f(\mathbf{A}) \propto \prod_{p=1}^P \mathbf{1}_{\mathbb{S}}(\boldsymbol{\alpha}_p). \quad (29)$$

The prior distributions for the endmember variances are conjugate inverse Gamma distributions with a common hyperparameter δ (as in (9)). A Jeffreys' prior is assigned to the hyperparameter δ as in (10).

V. MCMC ALGORITHM FOR ENDMEMBERS WITH DIFFERENT VARIANCES

As in the previous case, a hybrid Metropolis-within-Gibbs sampler will be used to generate samples asymptotically distributed according to the joint distribution of the abundance vectors and endmember variances. The sampler iteratively generates α_p according to $f(\alpha_p | \mathbf{y}_p, \sigma)$ for each pixel $p = 1, \dots, P$, σ_r^2 according to $f(\sigma_r^2 | \sigma_{-r}, \mathbf{Y}, \mathbf{A}, \delta)$ for each endmembers $r = 1, \dots, R$ (σ_{-r} denotes the variance vector σ whose r th component has been removed), and δ according to $f(\delta | \sigma)$.

A. Abundance generation

The conditional posterior distribution of the abundance vector α_p does not depend on the other pixels and is expressed as

$$f(\alpha_p | \mathbf{y}_p, \sigma) \propto \frac{1}{[c(\alpha_p)]^{L/2}} \exp\left[-\frac{\|\mathbf{y}_p - \mu(\alpha_p)\|^2}{2c(\alpha_p)}\right] \mathbf{1}_{\mathbb{S}}(\alpha_p). \quad (30)$$

Generating α_p according to this posterior is achieved with a Metropolis-within-Gibbs algorithm similar to the one described in paragraph III-A.

B. Variance generation

The generation according to $f(\sigma_r^2 | \sigma_{-r}, \mathbf{Y}, \mathbf{A})$ is achieved by R Metropolis-Hastings moves. Each Metropolis-Hastings move consists of drawing a variance σ_r^2 according to its conditional distribution

$$f(\sigma_r^2 | \sigma_{-r}, \mathbf{Y}, \mathbf{A}, \delta) \propto f(\mathbf{Y} | \mathbf{A}, \sigma) f(\sigma_r^2 | \nu, \delta)$$

with $\sigma_{-r} = [\sigma_1^2, \dots, \sigma_{r-1}^2, \sigma_{r+1}^2, \dots, \sigma_r^2]^T$. Introducing $c(\alpha_{-r}) = \sum_{i=1, i \neq r}^R \sigma_i^2 \alpha_i^2$ straightforward computations lead to (see Appendix A)

$$\begin{aligned} f(\sigma_r^2 | \sigma_{-r}, \mathbf{Y}, \mathbf{A}, \delta) &\propto \left(\frac{1}{\sigma_r^2}\right)^{\nu+1} \prod_{p=1}^P [\sigma_r^2 \alpha_{r,p}^2 + c(\alpha_{-r})]^{-L/2} \\ &\times \exp\left[-\sum_{p=1}^P \frac{\|\mathbf{y}_p - \mu(\alpha_p)\|^2}{2[\sigma_r^2 \alpha_{r,p}^2 + c(\alpha_{-r})]} - \frac{\delta}{\sigma_r^2}\right]. \end{aligned} \quad (31)$$

Sampling according (31) is achieved thanks to a Metropolis-Hastings step. The proposal distribution for this algorithm is an inverse Gamma distribution

$$\sigma_r^2 \sim \mathcal{IG}(\alpha_\sigma, \beta_\sigma), \quad (32)$$

where α_σ and β_σ are adjustable parameters. These parameters have been chosen in order to obtain the mean and the variance of the distribution (16), which improves the acceptance rate of the sampler.

C. Hyperparameter generation

The conditional distribution of the hyperparameter δ upon σ is the following Gamma distribution:

$$\delta|\sigma \sim \mathcal{G}\left(R, \sum_{r=1}^R \frac{1}{\sigma_r^2}\right). \quad (33)$$

A detailed step-by-step algorithm is presented in Algo. 2.

ALGORITHM 2:
Spectral unmixing using the NCM with different endmember variances.

- 1) Initialization:
 - Sample the hyperparameter $\delta^{(0)}$ from the pdf in Eq. (10),
 - Sample $\sigma^{(0)} = [\sigma_1^{2(0)}, \dots, \sigma_R^{2(0)}]$ from the pdf in Eq. (9),
 - For each pixel p , sample $\alpha^{(0)}$ according to a uniform distribution on \mathbb{S} ,
 - 2) Iterations: For $t = 1, 2, \dots$, do
 - For $p = 1, \dots, P$, sample $\alpha_p^{(t)}$ from the pdf in Eq. (30) using Metropolis-within-Gibbs,
 - For $r = 1, \dots, R$, sample $\sigma_r^{2(t)}$ from the pdf in Eq. (31) using Metropolis-within-Gibbs,
 - Sample $\delta^{(t)}$ from the pdf in Eq. (33),
-

VI. SIMULATION RESULTS ON SYNTHETIC DATA

This section illustrates the performance of the two proposed unmixing algorithms via simulations on synthetic data. The simulations have been conducted on pixels observed in $L = 276$ spectral bands ranging from wavelength $0.4\mu m$ to $2.5\mu m$ (from the visible to the near infrared).

A. NCM algorithm with a single endmember variance

The simulation depicted in this section have been obtained for the NCM algorithm introduced in Section III. A synthetic mixture of $R = 2$ endmembers is considered in this experiment. This trivial example has the advantage of having few parameters whose posteriors can be represented more easily. The means of these endmembers \mathbf{m}_1 and \mathbf{m}_2 have been extracted from the spectral libraries distributed with the ENVI package [16]. These spectra correspond to construction concrete and green grass and are depicted in Fig. 5. The endmember variance is

$\sigma^2 = 0.01$. The linear mixture considered in this section is defined by $\alpha^+ = [0.3, 0.7]^T$. Fig. 6 shows the posterior distributions of the abundances generated by the proposed Gibbs sampler with $N_{MC} = 25000$ iterations including $N_{bi} = 5000$ burn-in iterations². These distributions are in good agreement with the actual values of the abundances. Fig. 7 shows the estimated posterior distribution of σ^2 that is also in good agreement with the actual endmember variance $\sigma^2 = 0.01$.

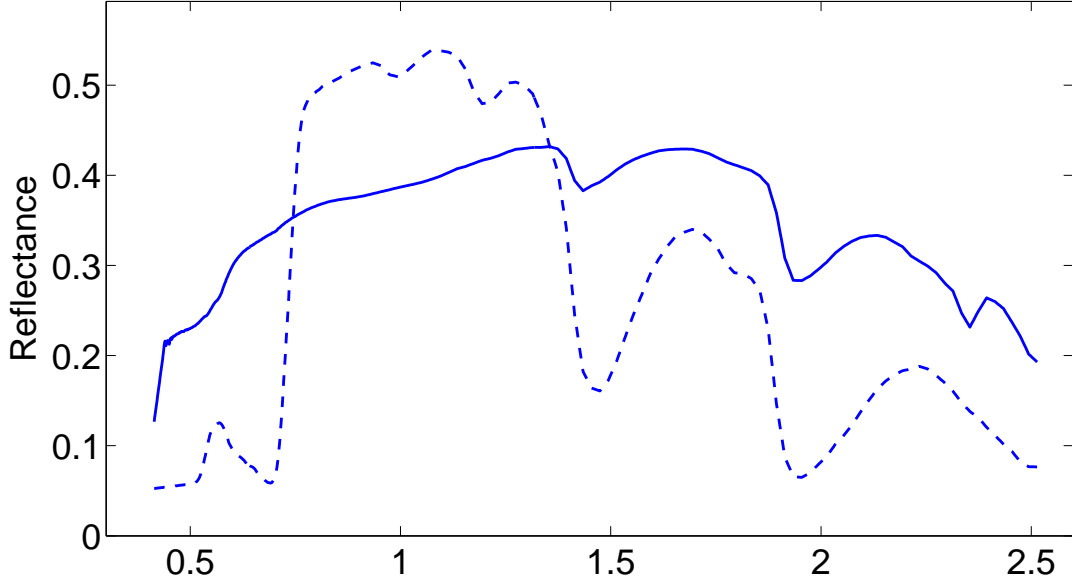


Fig. 5. Endmember spectra: construction concrete (solid line), green grass (dashed line).

The proposed Gibbs algorithm has been also tested for different values of the SNR. Fig. 8 shows the abundance MAP estimates of α_r and the corresponding standard deviations as a function of the SNR. It is important to mention here that the proposed Bayesian algorithm allows one to derive confidence intervals for the different estimates. These confidence intervals are computed from the samples generated by the Gibbs sampler. Note that the SNRs of the actual spectrometers like AVIRIS are not below 30dB when the water absorption bands have been removed [17]. The results in Fig. 8 indicate that the proposed Bayesian algorithm performs satisfactorily for these SNRs. Fig. 8 also shows that the proposed estimates of α_r converge (in

²Classically, the first samples generated by the Gibbs sampler (belonging to the so-called burn-in period) are not considered for parameter estimation.

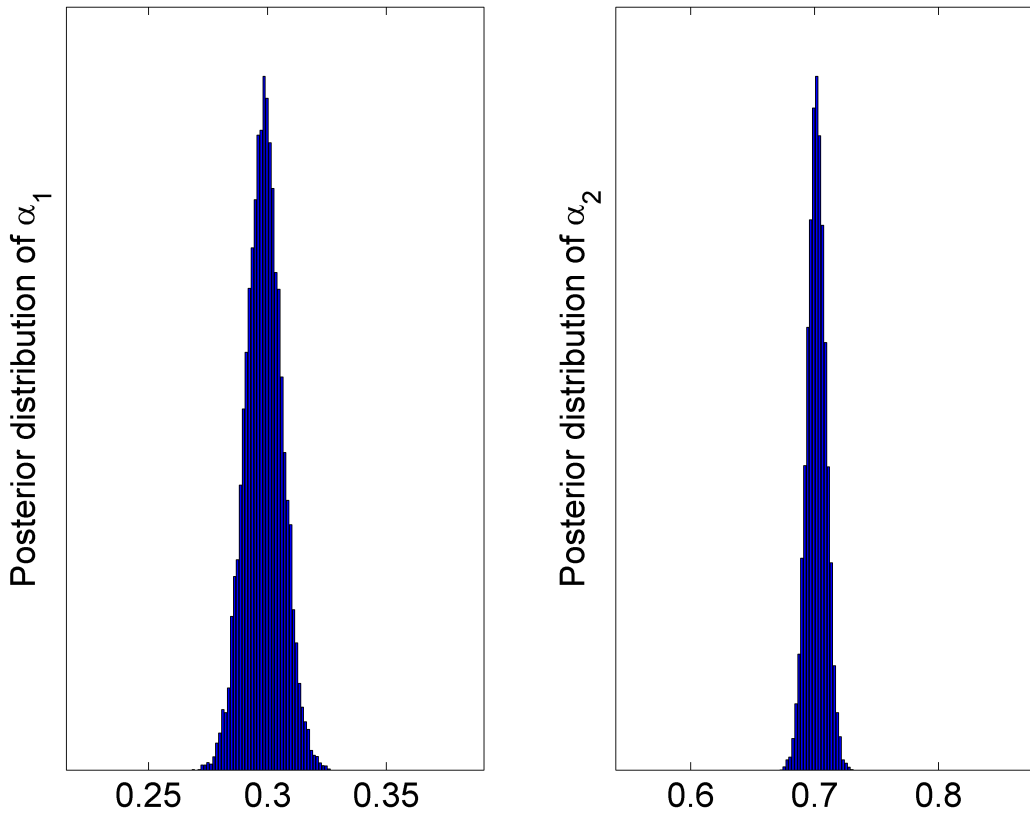


Fig. 6. Estimated posterior distributions of the abundances $[\alpha_1, \alpha_2]^T$.

the mean square sense) to the actual values of α_r when the SNR level increases.

B. NCM algorithm with different variances

The performance of the algorithm introduced in Section IV is illustrated with simulation results associated to synthetic data. In these simulations, $P = 3$ pixels have been generated by mixing $R = 3$ endmembers according (24). The actual parameter values are

- Pixel 1: $\boldsymbol{\alpha}_1^+ = [0.5, 0.3, 0.2]^T$, $\sigma_1^2 = 0.001$,
- Pixel 2: $\boldsymbol{\alpha}_2^+ = [0.4, 0.1, 0.5]^T$, $\sigma_2^2 = 0.006$,
- Pixel 3: $\boldsymbol{\alpha}_3^+ = [0.1, 0.3, 0.6]^T$, $\sigma_3^2 = 0.003$.

Fig. 9 shows the estimated posterior distributions of the variances σ_r^2 ($r = 1, \dots, R$) that are clearly centered around the actual values. The histograms of the abundances generated for each

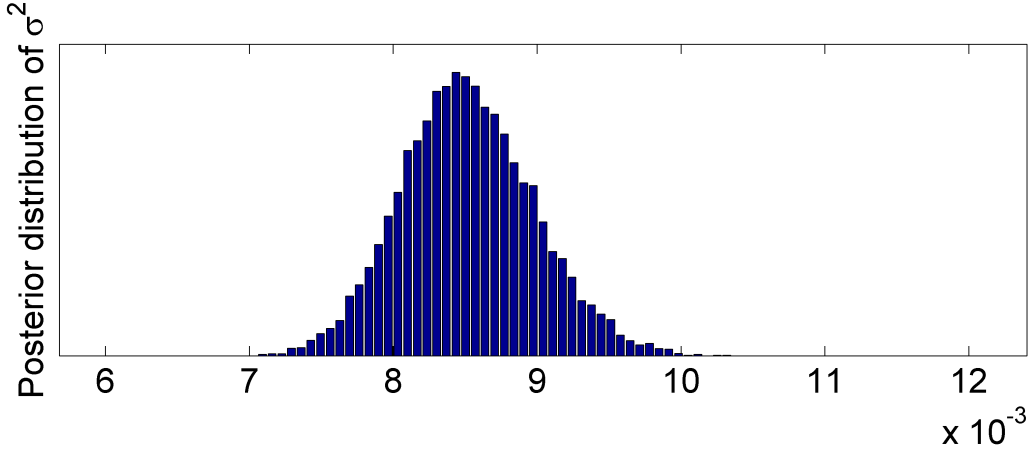


Fig. 7. Estimated posterior distribution of the variance σ^2 .

pixel by the proposed hybrid Gibbs sampler are depicted in Fig. 10. These results are in good agreement with the actual values of the abundances.

The performance of the algorithm based on different endmember variances (described in section IV) is compared to the algorithm based on a single endmember variance (described in section III). $P = 9$ synthetic pixels, generated according to the NCM with distinct variances, have been unmixed by the two different algorithms. The mean square errors (MSEs) of the abundance vectors are then computed for these algorithms using 100 Monte Carlo runs. Table I summarizes the corresponding results and shows that taking into account several variances allows one to improve the estimation performance for this example.

TABLE I
GLOBAL MSE OF THE ABUNDANCE VECTOR FOR THE NCM WITH UNIQUE VARIANCE AND WITH DISTINCT VARIANCES.

NCM with single variance	NCM with multiple variances
1.72×10^{-2}	1.54×10^{-2}

C. Comparison with other algorithms

This paragraph presents a comparison between the two algorithms developed in this paper and other strategies previously proposed in the literature. More precisely, we compare the following

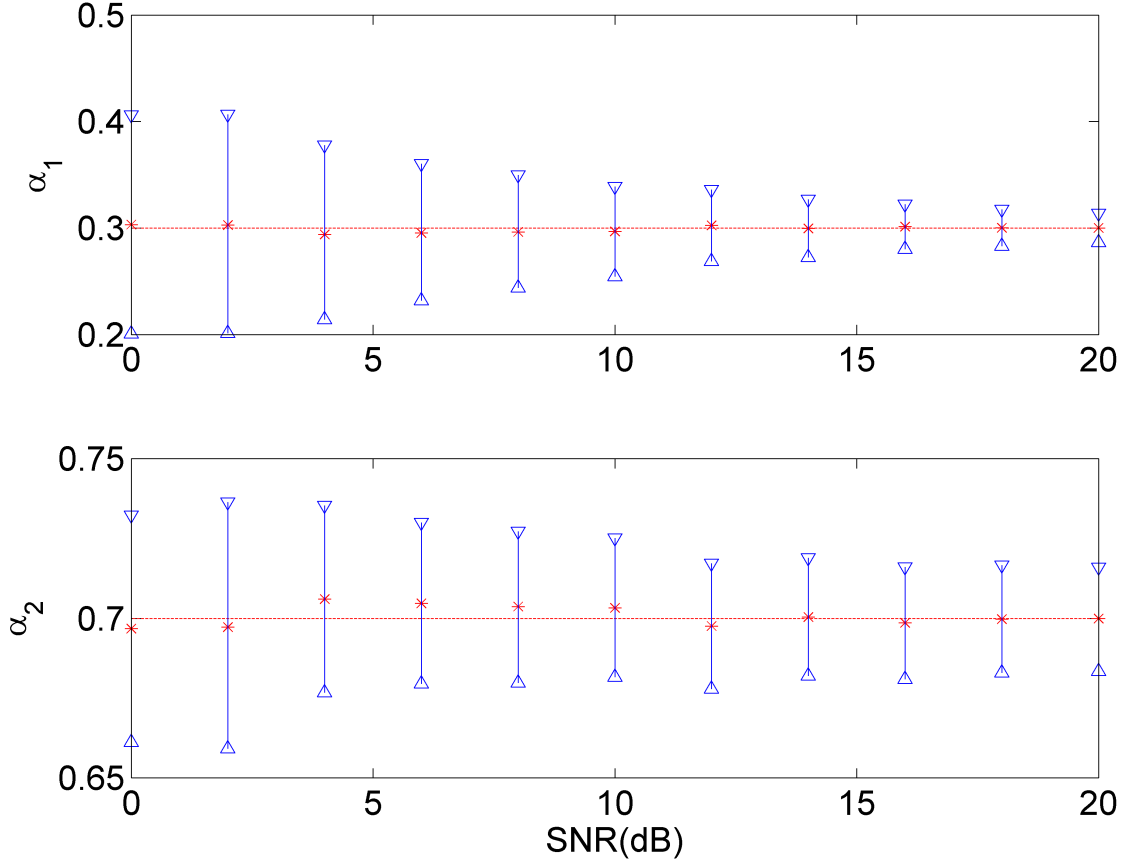


Fig. 8. MAP estimates (cross) and standard deviations (vertical bars) of the components of α^+ versus SNR.

unmixing strategies:

- the proposed Bayesian NCM algorithm presented in Sections II,
- a Bayesian algorithm derived from the LMM [7],
- the fully constrained least-squares (FCLS) method [18],
- the minimum volume constrained nonnegative matrix factorization (MVC-NMF) [19],
- the non-negative Independent Component Analysis (NN-ICA) [20],

The Bayesian NCM and the LMM-based algorithms of [7] and [18] are coupled with the VCA algorithm as an endmember extraction algorithm (EEA). Note that any other standard EEA (such as N-FINDR and pixel purity index [21]) could have been used in place of VCA. $P = 625$ synthetic pixels are generated according to the LMM with $R = 6$ endmembers, corrupted by an

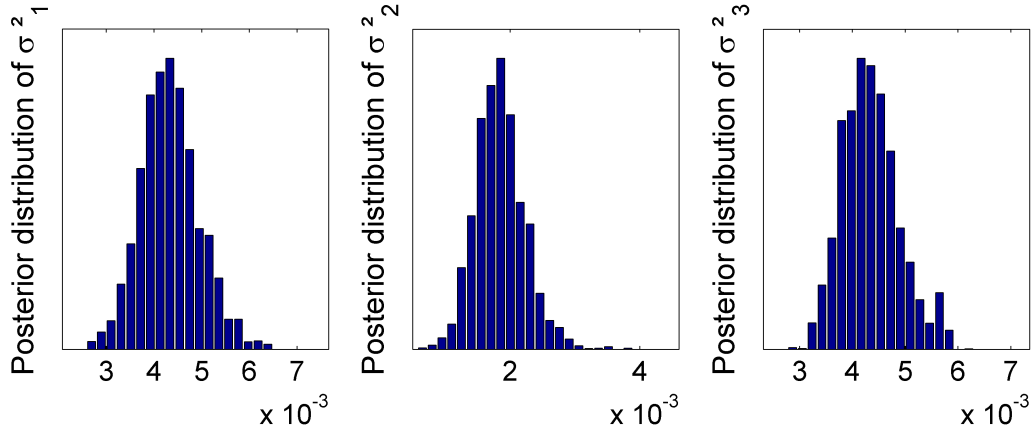


Fig. 9. Estimated posterior distribution of the variances for $P = 3$ pixels.

additive Gaussian noise leading to a signal-to-noise ratio (SNR) equal to 20dB. To evaluate the robustness of the NCM to the absence of pure pixels, the observations close to the endmember means (i.e., such that $\frac{1}{L} \|\mathbf{y}_p - \mathbf{m}_r\|^2 < \delta$, $\forall p, r$, with $\delta = 6.0 \times 10^{-2}$) have been removed from the synthetic image. The global MSE of the r th estimated abundance is defined as

$$\text{MSE}_r^2 = \frac{1}{P} \sum_{p=1}^P (\hat{\alpha}_{r,p} - \alpha_{r,p})^2 \quad (34)$$

where $\hat{\alpha}_{r,p}$ denotes the MMSE estimate of the abundance $\alpha_{r,p}$. Table II shows the global MSEs for the five different unmixing strategies mentioned before (Bayesian NCM, Bayesian LMM, FCL, MVC-NMF and NN-ICA). The proposed Bayesian NCM algorithm performs significantly better than the other unmixing algorithms. The improved performance obtained with the NCM is due to the robustness of this model (when compared to the usual LMM) to the absence of pure pixels in the image.

As a complementary study for this set of pixels, the global reconstruction error defined by

$$e = \sqrt{\frac{1}{P} \sum_{p=1}^P \|\mathbf{y}_p - \mathbf{M}\hat{\boldsymbol{\alpha}}_p^+\|^2} \quad (35)$$

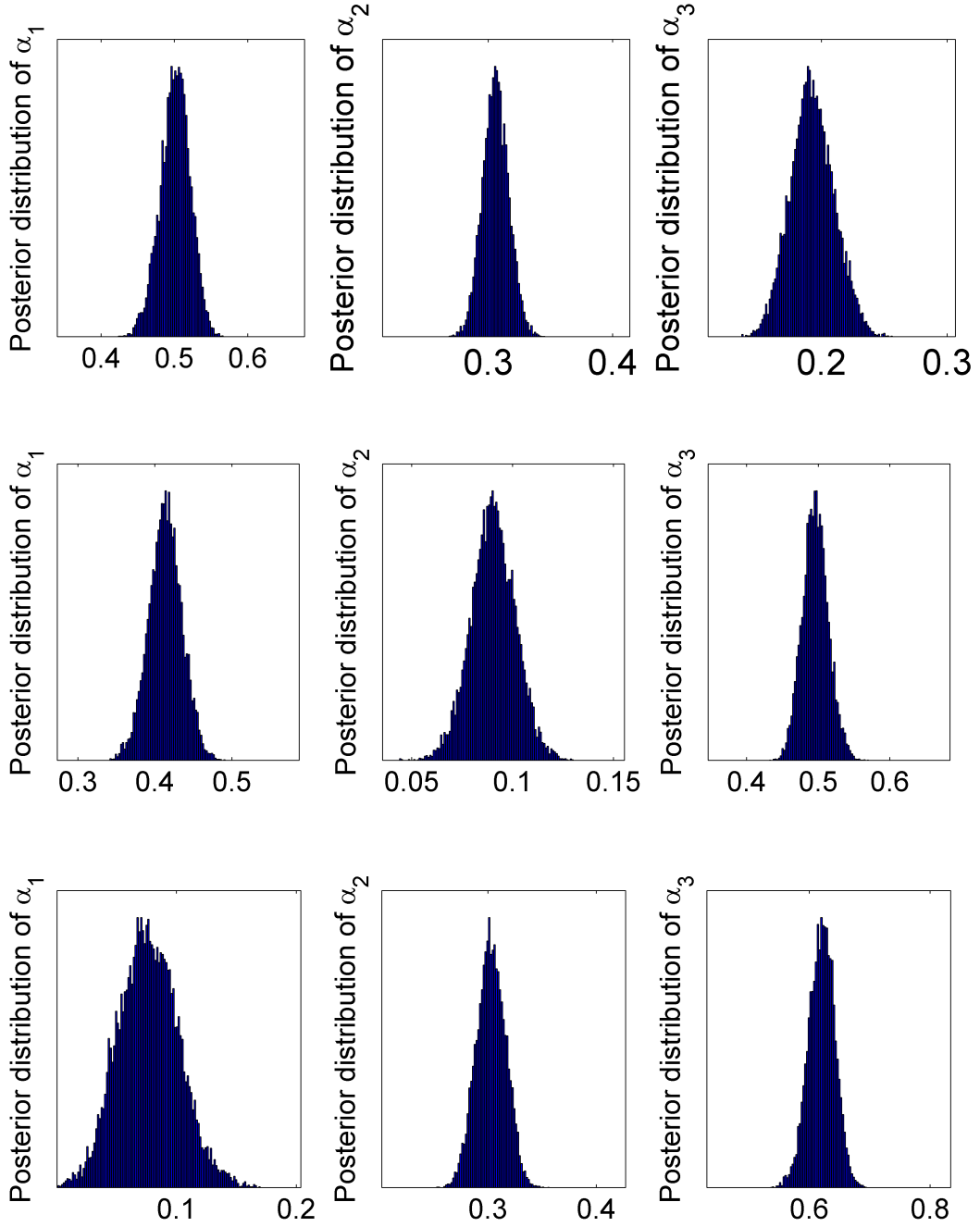


Fig. 10. Estimated posterior distributions of the abundances for each pixel (top: pixel 1, center: pixel 2, bottom: pixel 3).

is reported in Table III for the Bayesian NCM, the Bayesian LMM and the FCLS algorithms³. Note that the Bayesian LMM and FCLS algorithms require the *a priori* knowledge of determin-

³The MVC-NMF and NN-ICA algorithms have not been considered for this comparison since they estimate the endmembers and abundances jointly. Thus, small reconstruction errors for these algorithms do not indicate a good spectral unmixing.

TABLE II

GLOBAL MSEs EACH ABUNDANCE COMPONENT FOR DIFFERENT UNMIXING ALGORITHMS ($\times 10^{-3}$).

	Bayesian NCM	Bayesian LMM	FCLS	MVC-NMF	NN-ICA
MSE ₁ ²	7.8	13	9.1	7.7	18.2
MSE ₂ ²	9.6	10.4	9.9	24.1	41.4
MSE ₃ ²	8.5	23.2	10.2	45.4	45.2
MSE ₄ ²	8.2	15.9	8.8	26.2	45.3
MSE ₅ ²	10.2	14.8	11.5	12.5	46.8
MSE ₆ ²	10.8	11.7	11.5	35.6	44.9

istic endmembers $\mathbf{m}_1, \dots, \mathbf{m}_R$ contained in the matrix \mathbf{M} . Consequently, the actual endmember matrix \mathbf{M} is also used for computing the reconstruction error associated to the NCM algorithm for fair comparison. As shown in Table III, the Bayesian NCM yields the smaller reconstruction error.

TABLE III

RECONSTRUCTION ERRORS FOR THE BAYESIAN NCM, THE BAYESIAN LMM AND THE FCLS ALGORITHMS.

	NCM	LMM	FCLS
e	1.26	1.32	1.28

VII. SPECTRAL UNMIXING OF AN AVIRIS IMAGE

This section considers a real hyperspectral image of size 50×50 depicted in Fig. 11 to evaluate the performance of the different algorithms. This image has been extracted from a larger image acquired in 1997 by the Airborne Visible Infrared Imaging Spectrometer (AVIRIS) over Moffett Field, CA. The data set has been reduced from the original 224 bands to $L = 189$ bands by removing water absorption bands. First, the image has been pre-processed by a PCA to determine the number of endmembers present in the scene as explained in [1]. Then, the N-FINDR algorithm has been applied to this image to estimate the endmember spectra. The

$R = 3$ extracted endmembers (shown in Fig.12) correspond to vegetation, water and soil, and have been used as the mean vectors \mathbf{m}_1 , \mathbf{m}_2 and \mathbf{m}_3 .

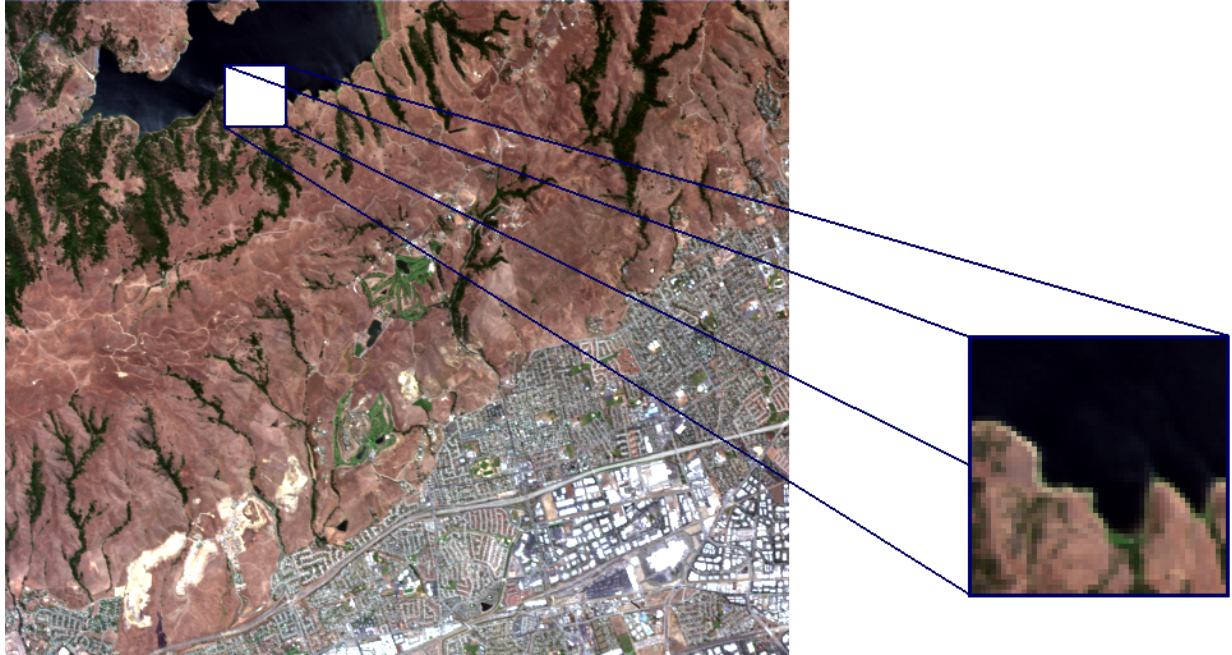


Fig. 11. Real hyperspectral data: Moffett field acquired by AVIRIS in 1997 (left) and the region of interest shown in true colors (right).

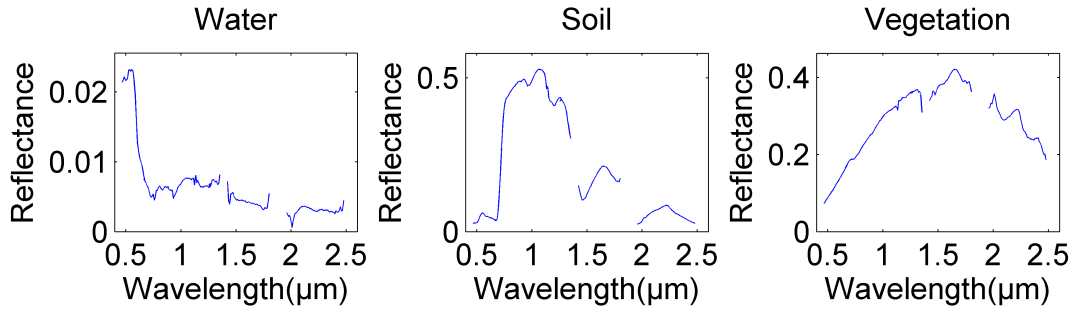


Fig. 12. The $R = 3$ endmember spectra obtained by the N-FINDR algorithm.

A. NCM algorithm with a single endmember variance

The image fraction maps estimated by the algorithm proposed in Sections II and III (for the $R = 3$ pure materials) are depicted in Fig. 13 (bottom). Note that a white (resp. black) pixel in

the map indicates a large (resp. small) value of the abundance coefficient. Thus, the lake area (represented by white pixels in the water fraction map and by black pixels in the other maps) can be clearly recovered. As depicted in Fig. 13, the fraction maps obtained with the three algorithms are clearly in good agreement. Other results given by the MVC-NMF [19] and the NN-ICA [20] are detailed in Fig. 14. The endmembers estimated by these methods (represented Fig. 15) does not exactly match with water, soil and vegetation. This explain why some maps are very different from those computed with the previous methods, e.g., the Bayesian NCM algorithm.

Some results regarding the estimation of the endmember variance σ^2 are also presented. Fig. 16 shows the estimated posterior distributions of σ^2 for the pixels #(35, 43) (left) and #(43, 35) (right) of the image as well as their MAP estimates.

The proposed Bayesian algorithm can be used to estimate the probability of endmember presence defined as $P[\alpha_i > \eta | \mathbf{m}_i]$, where η is a given threshold. Three distinct zones of 6×6 pixels, depicted in Fig.17, have been analyzed to estimate these probabilities. The first region (zone 1) has been extracted from the lake area and thus contains a majority of water pixels. Conversely, the other two regions (zones 2 and 3) are coastal areas containing soil and vegetation. Table IV shows the result obtained for different thresholds in each analyzed area.

TABLE IV
PROBABILITY OF PRESENCE FOR EACH ENDMEMBER.

	Zone 1 $\eta = 0.98$	Zone 2 $\eta = 0.9$	Zone 3 $\eta = 0.8$
$P[\alpha_{\text{water}} > \eta \mathbf{m}_{\text{water}}]$	0.9922	0	0
$P[\alpha_{\text{soil}} > \eta \mathbf{m}_{\text{soil}}]$	0	0.5147	0.0556
$P[\alpha_{\text{vegetation}} > \eta \mathbf{m}_{\text{veg.}}]$	0	0	0.2774

B. NCM algorithm with distinct endmember variances

This hyperspectral image has also been analyzed by the algorithm detailed in section IV to evaluate its performance. As the algorithm requires more than one pixel, the image has been

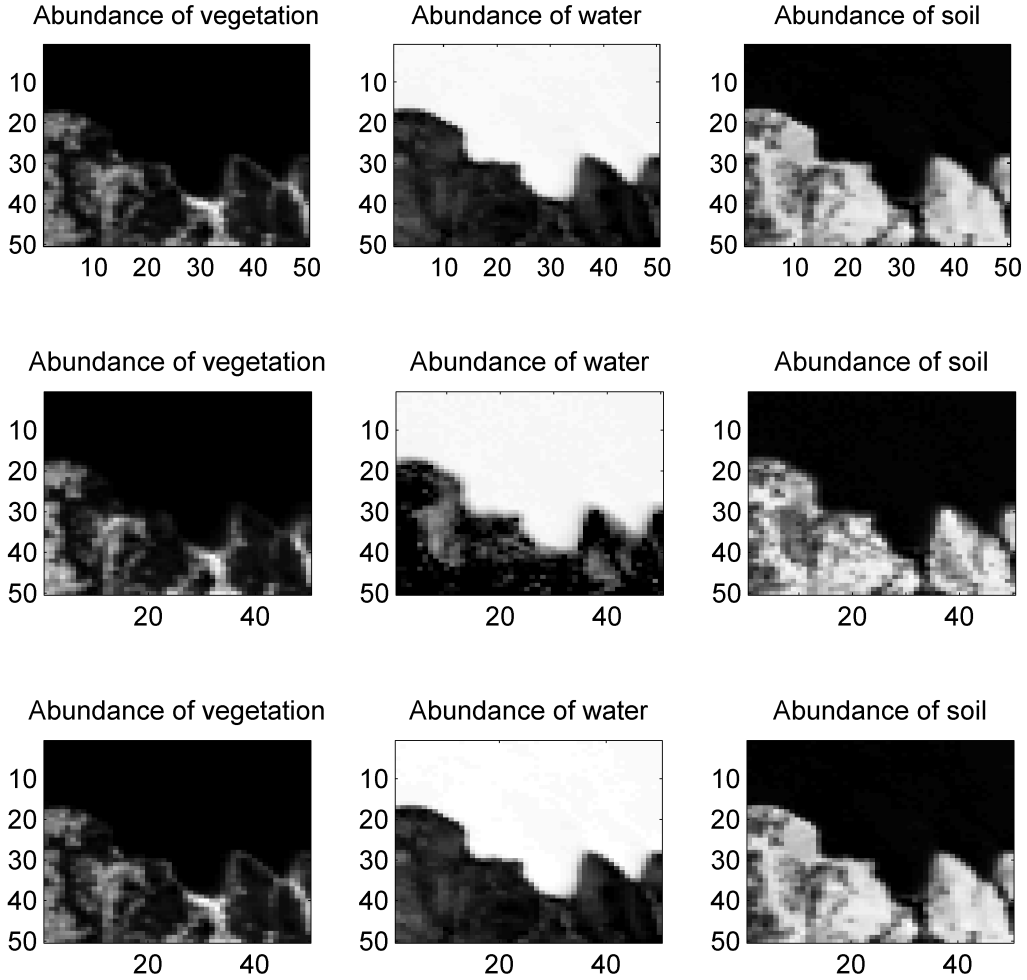


Fig. 13. Top: fraction maps estimated by the LMM algorithm (from [7]). Middle: fraction maps estimated by the FCLS algorithm [18]. Bottom: fraction maps estimated by the proposed algorithm (black (resp. white) means absence (resp. presence) of the material).

divided into 256 blocks of 3×3 pixels. Thus, the analyzed area⁴ has been reduced to 48×48 . The estimated variances for the endmembers associated to the block centered around the pixel #(35, 43) are shown in Table V. These results indicate that the variances can be estimated with good performance.

⁴Only the right and bottom edges of the image are not studied, which is a very small area compared to the full size of the image.

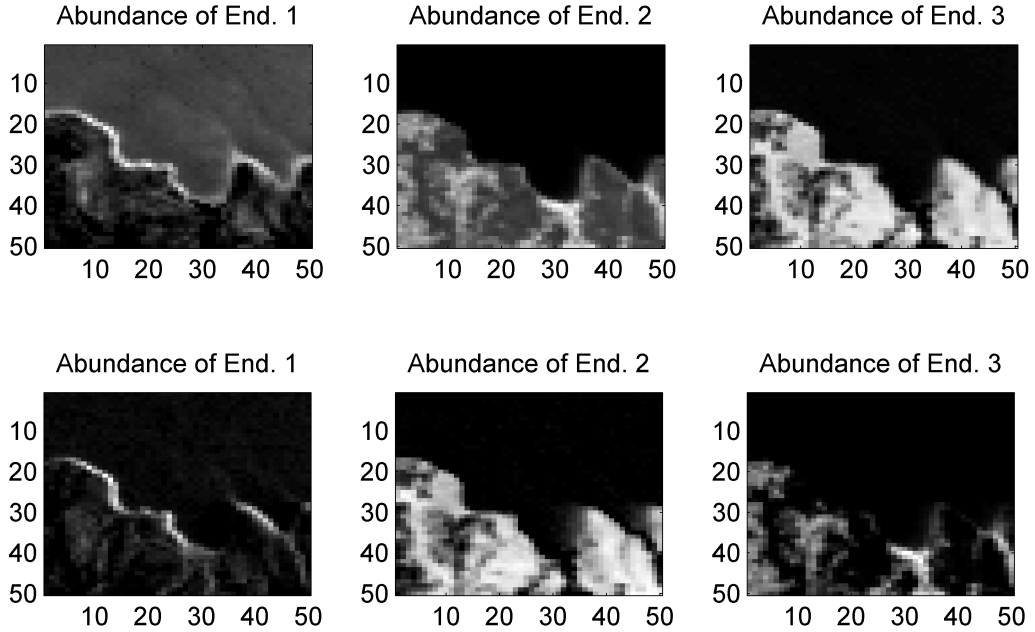


Fig. 14. Top: fraction maps estimated by the MVC-NMF algorithm (from [19]). Bottom: fraction maps estimated by the NN-ICA algorithm [20] (black (resp. white) means absence (resp. presence) of the material).

TABLE V
MMSE ESTIMATE OF σ_r^2 ($r = 1, \dots, R$).

	Soil	Vegetation	Water
MMSE estimates	1×10^{-4}	6.9×10^{-3}	1×10^{-4}

VIII. CONCLUSION

A new hierarchical Bayesian unmixing algorithm was derived for hyperspectral images. This algorithm was based on the normal compositional model introduced by Eismann and Stein [4]. The proposed algorithm generated samples distributed according to the joint posterior of the abundances, the endmembers variances and one hyperparameter. These samples were then used to estimate the parameters of interest. The proposed algorithm has several advantages versus the standard LMM-based algorithms. In particular, it allows one to extend the standard model to the case where endmember spectra have different variances. The simulation results on synthetic and

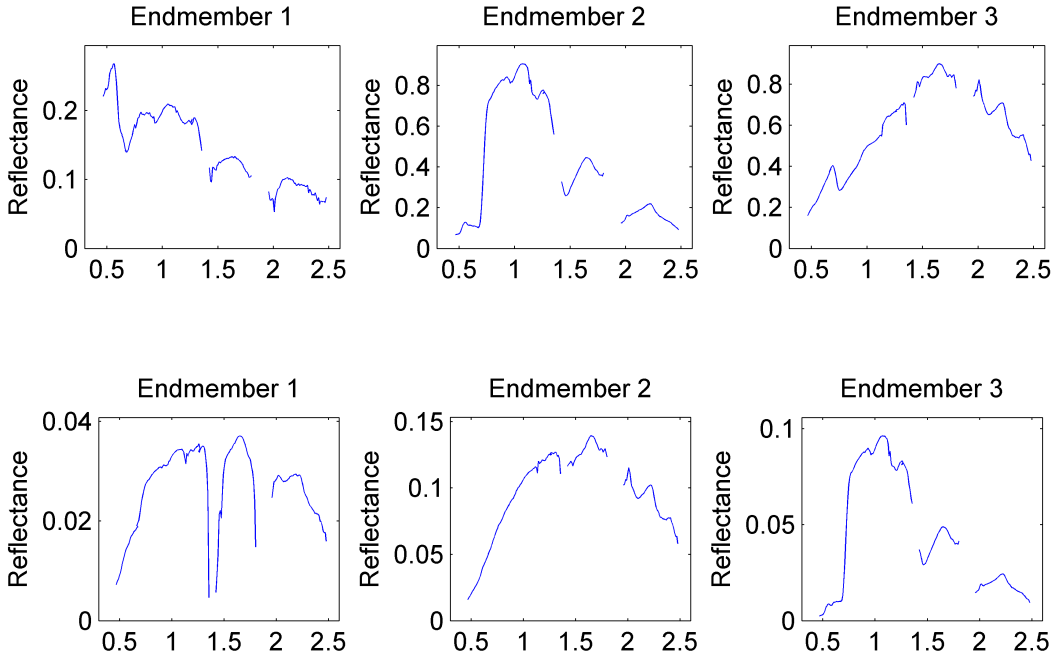


Fig. 15. Top: the $R = 3$ endmember spectra obtained by the MVC-NMF algorithm [19]. Bottom: the endmember spectra obtained by the NN-ICA algorithm [20].

real data showed very promising results.

Perspectives include the generalization of the NCM algorithm to more advanced models. For instance, the hyperspectral images could be considered as a set of homogenous regions surrounded by sharp boundaries. In this case, neighborhood conditions for the abundances could be introduced to improve unmixing.

APPENDIX A

$$\text{POSTERIOR DISTRIBUTION } f(\sigma_r^2 | \boldsymbol{\sigma}_{-r}, \mathbf{Y}, \mathbf{A}, \mathbf{M})$$

By using the Bayes' theorem, the posterior distribution $f(\sigma_r^2 | \boldsymbol{\sigma}_{-r}, \mathbf{Y}, \mathbf{A}, \mathbf{M})$ can be written

$$f(\sigma_r^2 | \boldsymbol{\sigma}_{-r}, \mathbf{Y}, \mathbf{A}, \mathbf{M}) \propto f(\mathbf{Y} | \mathbf{A}, \boldsymbol{\sigma}, \mathbf{M}) f(\sigma_r^2 | \nu, \delta) \quad (36)$$

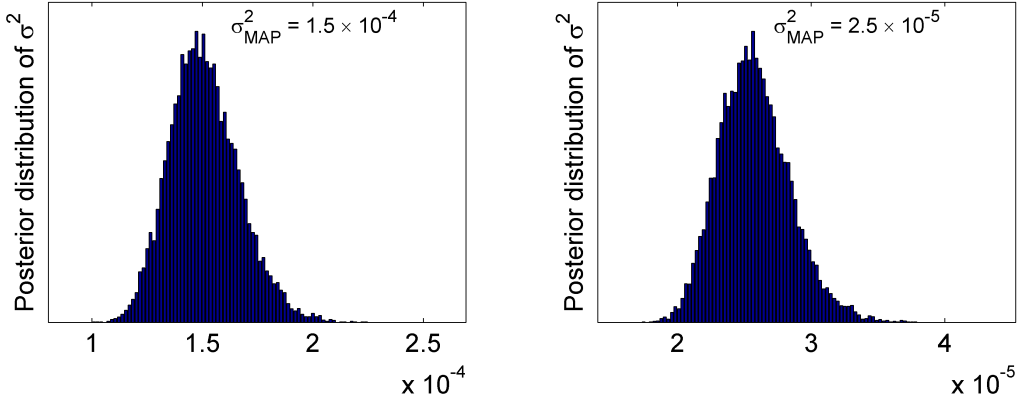


Fig. 16. Posterior distributions of the variance σ^2 for the pixels #35, 43 (left) and #43, 35 (right) estimated by the proposed algorithm.

which leads to

$$\begin{aligned} f(\sigma_r^2 | \boldsymbol{\sigma}_{-r}, \mathbf{Y}, \mathbf{A}, \mathbf{M}) &\propto \prod_{p=1}^P \left(\frac{1}{c(\boldsymbol{\alpha}_p)} \right)^{L/2} \\ &\times \exp \left(- \sum_{p=1}^P \frac{\|\mathbf{y}_p - \boldsymbol{\mu}(\boldsymbol{\alpha}_p)\|^2}{2c(\boldsymbol{\alpha}_p)} \right) \\ &\times \left(\frac{1}{\sigma_r^2} \right)^{\nu+1} \exp \left(- \frac{\delta}{\sigma_r^2} \right) \end{aligned}$$

This conditional posterior distribution can be rewritten

$$\begin{aligned} f(\sigma_r^2 | \boldsymbol{\sigma}_{-r}, \mathbf{Y}, \mathbf{A}, \mathbf{M}) &\propto \left(\frac{1}{\sigma_r^2} \right)^{\nu+1} \prod_{p=1}^P (\sigma_r^2 \alpha_{r,p}^2 + c(\boldsymbol{\alpha}_{-r}))^{-L/2} \\ &\times \exp \left(- \sum_{p=1}^P \frac{\|\mathbf{y}_p - \boldsymbol{\mu}(\boldsymbol{\alpha}_p)\|^2}{2(\sigma_r^2 \alpha_{r,p}^2 + c(\boldsymbol{\alpha}_{-r}))} - \frac{\delta}{\sigma_r^2} \right). \quad (37) \end{aligned}$$

REFERENCES

- [1] N. Keshava and J. Mustard, "Spectral unmixing," *IEEE Signal Process. Magazine*, pp. 44–56, Jan. 2002.
- [2] M. E. Winter, "Fast autonomous spectral endmember determination in hyperspectral data," in *Proc. 13th Int. Conf. on Applied Geologic Remote Sensing*, vol. 2, Vancouver, April 1999, pp. 337–344.
- [3] J. M. Nascimento and J. M. Bioucas-Dias, "Vertex component analysis: a fast algorithm to unmix hyperspectral data," *IEEE Trans. Geosci. and Remote Sensing*, vol. 43, no. 4, pp. 898–910, April 2005.

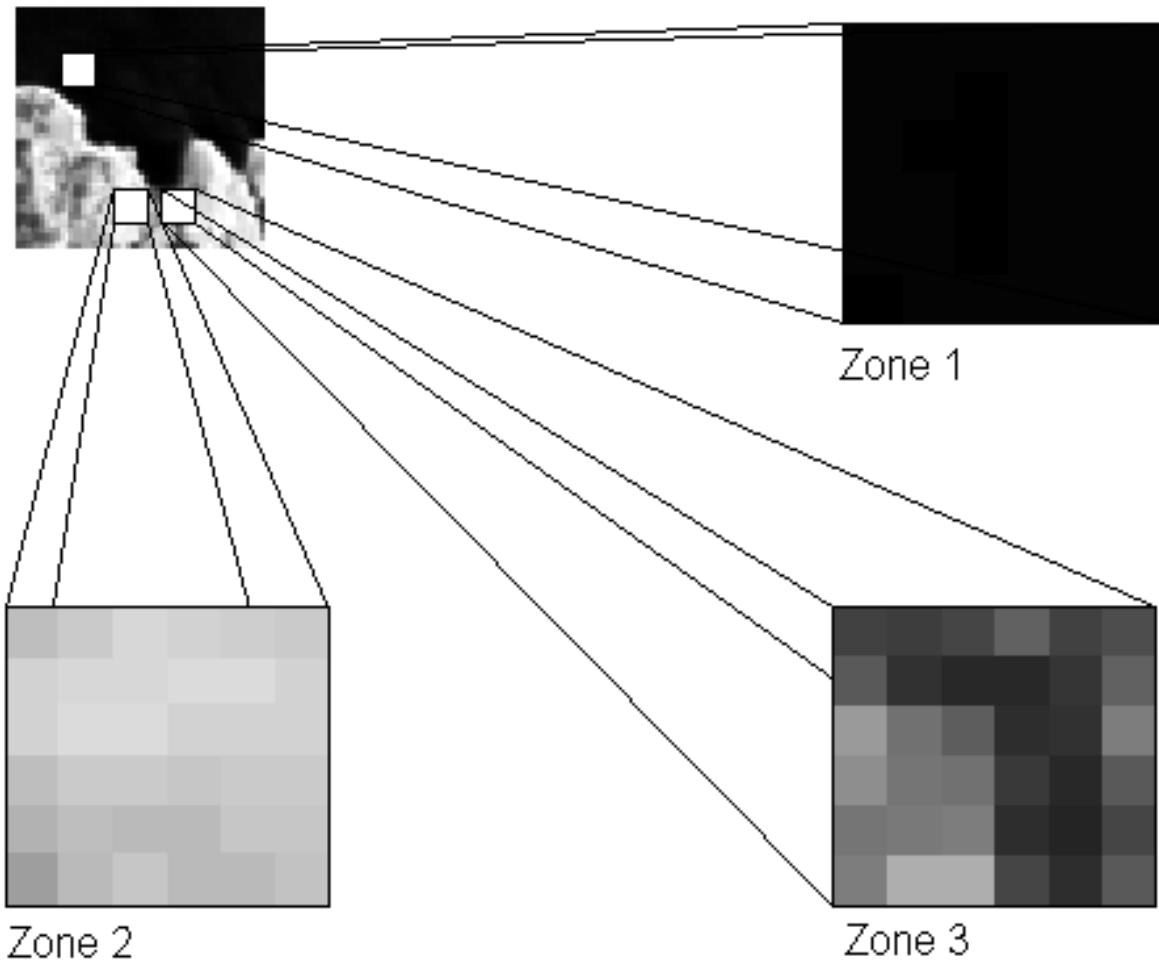


Fig. 17. Areas of water, soil and vegetation analyzed for the probability of presence.

- [4] M. T. Eismann and D. Stein, "Stochastic mixture modeling," in *Hyperspectral Data Exploitation: Theory and Applications*, C.-I. Chang, Ed. Wiley, 2007, ch. 5.
- [5] J. Settle, "On the relationship between spectral unmixing and subspace projection," *IEEE Trans. Geosci. and Remote Sensing*, vol. 34, no. 4, pp. 1045–1046, July 1996.
- [6] D. Manolakis, C. Siracusa, and G. Shaw, "Hyperspectral subpixel target detection using the linear mixing model," *IEEE Trans. Geosci. and Remote Sensing*, vol. 39, no. 7, pp. 1392–1409, July 2001.
- [7] N. Dobigeon, J.-Y. Tourneret, and C.-I Chang, "Semi-supervised linear spectral using a hierarchical Bayesian model for hyperspectral imagery," *IEEE Trans. Signal Processing*, vol. 56, no. 7, pp. 2684–2696, July 2008.
- [8] C. P. Robert and G. Casella, *Monte Carlo Statistical Methods*, 2nd ed. New York: Springer Verlag, 2004.
- [9] D. Stein, "Application of the normal compositional model to the analysis of hyperspectral imagery," in *Proc. IEEE Workshop on Advances in Techniques for Analysis of Remotely Sensed Data*, Oct. 2003, pp. 44–51.
- [10] J. Diebolt and E. H. S. Ip., "Stochastic EM: method and application," in *Markov Chain Monte Carlo in Practice*, W. R.

- Gilks, S. Richardson, and D. J. Spiegelhalter, Eds. London: Chapman & Hall, 1996.
- [11] S. Moussaoui, H. Hauksdóttir, F. Schmidt, C. Jutten, J. Chanussot, D. Brie, S. Douté, and J. A. Benediksson, “On the decomposition of mars hyperspectral data by ICA and Bayesian positive source separation,” *Neurocomputing*, vol. 71, no. 10-12, pp. 2194–2208, 2008.
 - [12] N. Bali and A. Mohammad-Djafari, “Bayesian approach with hidden markov modeling and mean field approximation for hyperspectral data analysis,” *IEEE Trans. Image Processing*, vol. 17, no. 2, pp. 217–225, 2008.
 - [13] H. Snoussi, “Efficient bayesian spectral matching separation in noisy mixtures,” *IEEE Trans. Image Processing*, to appear.
 - [14] E. Punskaya, C. Andrieu, A. Doucet, and W. Fitzgerald, “Bayesian curve fitting using MCMC with applications to signal segmentation,” *IEEE Trans. Signal Processing*, vol. 50, no. 3, pp. 747–758, March 2002.
 - [15] N. Dobigeon, J.-Y. Tourneret, and M. Davy, “Joint segmentation of piecewise constant autoregressive processes by using a hierarchical model and a Bayesian sampling approach,” *IEEE Trans. Signal Processing*, vol. 55, no. 4, pp. 1251–1263, April 2007.
 - [16] RSI (Research Systems Inc.), *ENVI User’s guide Version 4.0*, Boulder, CO 80301 USA, Sept. 2003.
 - [17] R. O. Green *et al.*, “Imaging spectroscopy and the airborne visible/infrared imaging spectrometer (AVIRIS),” *Remote Sens. Environ.*, vol. 65, no. 3, pp. 227–248, Sept. 1998.
 - [18] D. C. Heinz and C.-I Chang, “Fully constrained least squares linear spectral mixture analysis method for material quantification in hyperspectral imagery,” *IEEE Trans. Geosci. and Remote Sensing*, vol. 39, no. 3, pp. 529–545, March 2001.
 - [19] L. Miao and H. Qi, “Endmember extraction from highly mixed data using minimum volume constrained nonnegative matrix factorization,” *IEEE Trans. Geosci. and Remote Sensing*, vol. 45, no. 3, pp. 765–776, March 2007.
 - [20] M. D. Plumley and E. Oja, “A “nonnegative-PCA” algorithm for independent component analysis,” *IEEE Trans. Neural Netw.*, vol. 15, no. 1, pp. 66–76, Jan. 2004.
 - [21] J. W. Boardman, F. A. Kruse, and R. O. Green, “Mapping target signatures via partial unmixing of aviris data,” in *Summaries of Fifth Annual JPL Airborne Earth Science Workshop*, R. O. Green, Ed. JPL Publication, 1995, pp. 23–26.